# Modelling, Identification and Experimental Validation of a Hydraulic Manipulator Joint for Control

Glen Bilodeau
gbilod@cim.mcgill.ca

Evangelos Papadopoulos
egpapado@cim.mcgill.ca

Department of Mechanical Engineering & Centre for Intelligent Machines
McGill University
Montreal, QC, Canada H3A 2A7

**Abstract**

*In this paper, modelling and identification of a hydraulic servoactuator system is presented. The development of the model is important for further understanding the system and for developing a robust force controller. A systems approach is used to model the various subsystems including the servovalve dynamics, fluid dynamics and the vane and load dynamics. Included in the model are line losses, leakage, and hysteresis. System parameters are identified using the elbow joint of the SARCOS slave experimental hydraulic manipulator. Specialized hardware was designed and constructed for this purpose. The model was validated by comparing simulation and experimental results. The correlation between model and actual system response proved to be very good. Hence, the developed model predicts well system dynamic behavior and will prove useful in the development of a robust force controller.*

## 1: Introduction

Many tasks that require humans to interact with their environment, either through direct contact or via a tool, may pose a danger to complete due to precarious work location or environmental conditions. For example, some applications include hazardous waste management, under-water operations, fire-fighting and live-line maintenance.

Teleoperation or automation of such tasks would distance humans from dangerous sites reducing risk of injury and would increase efficiency. However, the control of manipulators interacting with an environment is very complex due to several factors. The manipulator may be located on a vehicle or on a long boom and the manipulator itself may demonstrate some degree of flexibility due to actuator, sensor and link dynamics. Also, a particular task may require large forces to be transmitted to the environment. Of special interest are manipulators with hydraulic actuators, due to their high force output to weight ratio, their inertance to fire hazards and the availability of hydraulic power in mobile applications.

Hydraulic actuators further complicate the control of manipulators in contact with their environment. Unlike electrical actuators in which a current produces a torque, a current input to a hydraulic actuator modulates valve resistance. Thus, the direct control of torque is not as easily accomplished. In order to provide an effective and robust control of the interaction between a hydraulic manipulator and its environment, a dynamic model of the robot's joints is required. In turn, a model will be useful in the development, simulation and implementation of a controller for a hydraulic manipulator.

The majority of prior work in automation or teleoperated control of manipulators deals with electrically actuated manipulators. In terms of hydraulic actuators, comparatively less work has been done. Previous research has spanned both modelling and control of hydraulic actuators. With respect to modelling, some works deal with the traditional spool valve, for which the orifice areas are generally linear with respect to the valve position. In contrast, the servovalve used in this work is of the jet-pipe/suspension type which is more complex. One advantage of this type of servovalve is that there is no contact between surfaces as there is between the spool and the spool housing. Another advantage is that these valves can be very fast due to their small moving mass. For the jet-pipe servovalve, a detailed model is proposed and studied in [4] and [12].

In terms of control of hydraulic actuators, modelling physical effects is important. In previous works, position and force control have been studied. A linearized model was used for position control of a spool-valve and rotary actuator system, [9]. A model was used in a feedforward simulation filter for control of a hydraulically actuated flexible manipulator, [10]. In force control, several algorithms in the hybrid position/force control have been developed using a model-based approach, [3], [6], and [14]. Explicit force control algorithms for hydraulic actuators have been demonstrated in [4] and [11]. The impedance control law, which is model-based, was applied to a hydraulic manipulator in [8]. Although the focus is on control, modelling is essential in understanding the system to be controlled. One way of obtaining a faithful and robust controller is to include a model-based portion in order to reduce control effort.

This paper deals with the accurate modelling of the elbow joint of a small slave SARCOS dexterous manipulator with the goal of using this model for control purposes. This model includes hysteresis, orifice areas,

damping, and leakage. To date, no model of a hydraulically actuated joint which includes servovalve and rotary actuator dynamics is available in the literature. The paper is organized as follows: in Section 2 the physical characteristics of the joint's subsystems are discussed. System equations are given. Section 3 describes the experimental setup and discusses the parameters identified and the procedures used. Section 4 compares experimental results with simulation results, validating the model. Finally, conclusions are given in Section 5.

## 2: System Modelling

Due to the highly non-linear nature of this hydraulic system, the possibility of instability and limited performance in control is high. Thus, a model of each subsystem will allow an accurate characterization of the system and a good prediction of the system's behavior. The hydraulic joint system is composed of a one-stage suspension type servovalve, hydraulic lines, a rotary actuator and a load. Each subsystem is shown in Figure 1. The bond graph of this system is given in a previous technical article [1]. In this section, the equations describing the dynamics of these subsystems are discussed. The end result is a set of first order nonlinear equations of the form

$$\dot{\boldsymbol{x}} = \boldsymbol{f(x,u)}, \quad \boldsymbol{y = g(x,u)} \tag{1}$$

First, consideration is given to the hysteresis effects in the servovalve. Second, the valve tip dynamics are described. Fluid dynamics are then discussed, along with the vane and load system equations.

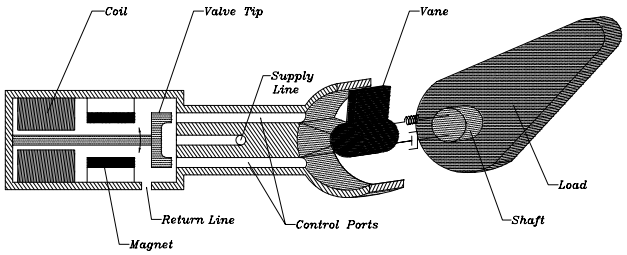


**Figure 1. Joint and Valve Schematic.**

### 2.1: Servovalve Hysteresis

An important phenomenon in the servovalve is hysteresis. In order to include the hysteresis model, an additional differential equation is added which requires, as input, the actual current and produces as output a virtual current, $i_{hys}$, which modulates the valve position.

To mathematically represent the phenomenon of hysteresis, a model based on the Jiles-Atherton theory for magnetization of ferromagnetic material is used, [5]. The model is suitable for insertion into system simulation. It accounts for major and minor loops with knowledge of only the switching point. For modelling purposes, we consider a one-to-one hysteresis between the current after hysteresis, $i_{hys}$, and the actual current. With the notation used in this paper, the formulation, derived from [5], is

$$\dot{i}_{hys} = \frac{\Lambda\mu_o \dot{i}\left(i_s L(i,i_{hys}) - i\right)}{k\delta - \mu_o\alpha\left(i_s L(i,i_{hys}) - i\right)} \tag{2}$$

where $L$, the Langevin function, and $\delta$ are given by

$$L(i,i_{hys}) = \coth\left(\mu_o(i+\alpha i_{hys})\right) - \frac{1}{\mu_o(i+\alpha i_{hys})}$$
$$\delta = sign\left(\dot{i}\right) \tag{3}$$

The scaling factor, $\Lambda$, which is less than unity for minor loop generation depends on the switching point and the major loop which saturates at $i_s = \pm 1$A. The parameters, $\mu_o$, $\alpha$, and $k$, affect the inclination and width of the hysteresis.

### 2.2: Valve Tip Dynamics

The servovalve consists of a moving element actuated by a small torque motor. An input current modulates the position of the valve tip opening supply and return orifices, allowing flow to enter and leave the actuator. The dynamics of the valve tip can be approximated by a second order lumped parameter system with mass, $m_v$, damping coefficient, $b_v$, and stiffness, $k_v$. Furthermore, as the valve tip moves, flow forces are generated due to a change in the direction of flow of the fluid. For the suspension type valve, a suitable physically based characterization of the flow is not available although an experimentally based model was proposed by [12]. The valve hysteresis is lumped into $i_{hys}$ as discussed in the previous section. Therefore, the dynamic equations of the valve tip in state space form is

$$\dot{x}_v = v_v$$
$$\dot{v}_v = \frac{1}{m_v}\left(Bi_{hys} + F_f - b_v v_v - k_v x_v\right) \tag{4}$$

The net effect of $i_{hys}$ is a hysteresis between the input current and the valve tip position, $x_v$. The hysteresis and valve tip equations, Eqs (2), (3), and (4) combine to characterize the behavior of the servovalve. Since the valve tip dynamics may be fast compared to other system dynamics, it may be ignored in the controller development, [7], but is included here for completeness.

### 2.3: Fluid Dynamics

From the schematic of the joint, Figure 1, four types of flows can be identified. These include flow through lines, flow through orifices, leakage flow and flow through the actuator. Line losses are represented as linear resistances. Fluid inertance due to fluid mass in the lines as well as fluid capacitance due to fluid compressibility are taken into account in the model, [2], [13]. The latter is significant as the fluid impinges on the vane of the rotary actuator.

Flow through an orifice is taken as turbulent. The relation between pressure drop across the orifice and the flow through it is represented by the square root law

$$Q = C_d A_{orifice}(x_v)\sqrt{\frac{2}{\rho}\left(P_{hi} - P_{lo}\right)}$$
$$= g_{orifice}\left(x_v, P_{hi}, P_{lo}\right) \tag{5}$$

where $C_d$ is the discharge coefficient. Now, consider leakages within the system. As shown in Figure 1, there is a clearance between the valve tip and the receiver. Two stages of leakage are evident. One leakage is from the

supply line, $P_{sv}$, directly to the return line, $P_{rl}$, as fluid traverses the clearance from supply to the valve tip where the pressure is denoted as $P_{sv2}$. The second stage occurs between $P_{sv2}$ and the two chamber pressures, $P_{p1}$ and $P_{p2}$, as the fluid traverses a second time the gap this time to the control ports, $P_{p1}$ and $P_{p2}$.

The flow through the actuator is related to the vane's angular velocity through the actuator volumetric displacement, $D_v$. Furthermore, for the rotary actuator, the leakage between chambers is taken into account and is assumed to be proportional to the load pressure. The leakage coefficient, or resistance, given as $R_v$, is dependent on fluid viscosity [2], but it is taken as a constant in this work.

With the notation of Table 1, the dynamic equations of the flow from servovalve to actuator are

$$\dot{Q}_{sv} = \frac{A_s}{\rho l_s}\left(P_s - \frac{128\mu l_s}{\pi d_s^4}Q_{sv} - P_{sv}\right) \tag{6}$$

$$\dot{P}_{sv} = \frac{1}{C_A}\left(Q_{sv} - g_{lk}(x_v, P_{sv}, P_{rl}) - g_v(x_v, P_{sv}, P_{sv2})\right) \tag{7}$$

$$\begin{aligned}\dot{P}_{p1} = \frac{\beta}{(V_{c1}+V_{p1})}\big(&g_1(x_v, P_{sv2}, P_{p1}) - g_4(x_v, P_{p1}, P_{rl}) \\ &- D_v\omega_{vn} - R_v(P_{p1} - P_{p2})\big)\end{aligned} \tag{8}$$

$$\begin{aligned}\dot{P}_{p2} = \frac{\beta}{(V_{c2}+V_{p2})}\big(&g_2(x_v, P_{sv2}, P_{p2}) - g_3(x_v, P_{p2}, P_{rl}) \\ &+ D_v\omega_{vn} + R_v(P_{p1} - P_{p2})\big)\end{aligned} \tag{9}$$

$$\dot{Q}_{rl} = \frac{A_r}{\rho l_r}\left(P_{rl} - \frac{128\mu l_r}{\pi d_r^4}Q_{rl} - P_r\right) \tag{10}$$

The two dependent variables, $P_{sv2}$ and $P_{rl}$, are cumbersome to solve for assuming the square root law. To simplify solution, linear resistances were assumed. They can be found through compatibility equations giving the following

$$P_{sv2} = w_1(P_{sv}, P_{p1}, P_{p2}, x_v, Q_{rl}) \tag{11}$$

$$P_{rl} = w_2(P_{sv}, P_{p1}, P_{p2}, x_v, Q_{rl}) \tag{12}$$

It can be noted that differences between this model and that of [12] include the leakage between chambers of the rotary actuator, whereas the focus of the previous work is a linear actuator. Also, there are two stages of leakage in the servovalve as discussed above. In the suspension type valve, the supply flow impinges the valve tip and is redirected to the control ports (see Figure 1). In addition, geometrically, the orifice areas as a function of the valve tip position differ from those studied in [12]. The configuration of the orifices is different due to a difference in servovalve design.

**Table 1. Nomenclature for Fluid Dynamics.**

| Variable | Definition |
|---|---|
| $\rho$, $\mu$, $\beta$ | density, viscosity and bulk modulus of oil. |
| $A_s$, $l_s$, $d_s$ | cross-sectional area, length and diameter of supply line. |
| $A_r$, $l_r$, $d_r$ | cross-sectional area, length and diameter of return line. |
| $P_s$, $P_r$ | pump pressure and tank pressure. |
| $Q_{sv}$, $P_{sv}$ | flow through supply line, supply pressure before servovalve. |
| $P_{sv2}$ | pressure at valve tip. |
| $Q_{rl}$, $P_{rl}$ | flow through return line, return pressure after servovalve. |
| $P_{p1}$, $P_{p2}$ | chamber pressures, port 1 and port 2. |
| $V_{p1}$, $V_{c1}$ | volume in line of port 1 and in chamber 1. |
| $V_{p2}$, $V_{c2}$ | volume in line of port 2 and in chamber 2. |
| $C_d$ | discharge coefficient. |
| $D_v$ | rotary actuator volumetric displacement. |
| $R_v$ | leakage coefficient of rotary actuator. |
| $C_A$ | accumulator capacitance. |

### 2.4: Vane and Load Dynamics

The actuator is a rotary vane type. The vane is modelled as a second order mechanical rotation system with input torque related to the load pressure through the actuator displacement, $D_v$. The friction between the vane and the actuator housing is modelled as Coulomb friction, denoted by $\tau_{coul}$, as well as viscous friction. Viscous friction was lumped into the damping term of the load. The load is connected via a shaft which is taken as non-rigid. Applying straightforward mechanical system analysis, the equations of motion for the vane and the load are given as

$$\begin{aligned}\dot{\omega}_{vn} = \frac{1}{J_v}\big(&D_v(P_{p1} - P_{p2}) - \tau_{coul}(\omega_{vn}) - b_{vn}\omega_{vn} \\ &- k_s(\theta_{vn} - \theta_l) - b_s(\omega_{vn} - \omega_l)\big)\end{aligned} \tag{13}$$

$$\begin{aligned}\dot{\omega}_l = \frac{1}{J_l}\big(&k_s(\theta_{vn} - \theta_l) + b_s(\omega_{vn} - \omega_l) - \tau_{coul}(\omega_l) \\ &- b_l\omega_l - W_l\sin(\theta_l) + \tau_{ext}\big)\end{aligned} \tag{14}$$

Here, $\omega_{vn}$ and $\omega_l$ are the vane and load angular velocities, $b_s$, $b_{vn}$, and $b_l$ are, respectively, the shaft, vane and load damping coefficients, while $k_s$ is the shaft stiffness. The vane and load rotary inertias are given by $J_v$ and $J_l$ respectively. Finally, the weight of the load is given by $W_l$ and external torques are represented by $\tau_{ext}$.

## 3: Identification of Parameters

Required model parameters were obtained with various methods. Some parameters were obtained from handbooks and manufacturer specifications such as loss coefficients and oil properties. However, other parameters needed to be obtained through experiments. First, a description of the experimental apparatus is given.

### 3.1: Apparatus

The high performance SARCOS hydraulic manipulator is used for the experimental determination and validation of the model parameters. For the joint model, the elbow of the slave manipulator is used. Sensors onboard the robot include an optical encoder angular position sensor, a rotary variable differential transformer (RVDT) for analog angular position measurement, and a strain-gage, full-bridge joint torque sensor.

Additional apparatus fabricated for identification of servovalve and actuator parameters include a steel brace to immobilize the elbow joint, three pressure transducers, a graduated cylinder, and a manifold equipped with pressure taps. The brace was designed and constructed for the study of the open-loop system in a static mode and can be used to validate static joint torque control, see Figure 2(a). The manifold was designed and built to allow access to the supply, return and the two control lines for pressure measurement, see Figure 2(b). For the manifold, the pressure transducers and the interface to the robot (middle right) are evident. By strategically blocking certain ports, a flow rate, such as actuator leakage, may be measured by volume measurements over time. The usefulness of the equipment is three-fold: (1) identification, (2) validation of the model, and (3) possible use of pressure signals in a feedback loop. In addition, the manifold may be installed at other joints with similar servovalve/robot interface.

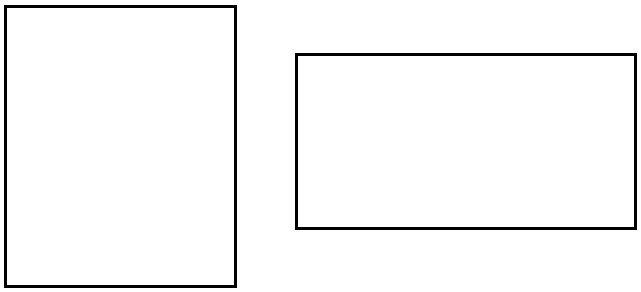

**(a)** **(b)**

**Figure 2. Apparatus: (a) Joint Brace; (b) Manifold.**

## 3.2: Experiments

Several experiments were performed to identify the key parameters of each subsystem. For brevity, only the experiments for identification of the servovalve dynamic parameters, the volumetric displacement of the actuator and the joint shaft stiffness will be discussed here. The procedure of the experiments was designed to isolate each subsystem and therefore the parameters of interest.

**3.2.1: Servovalve Parameters.** The key parameters of the servovalve are the geometry of the valve tip and the dynamic characteristics of the valve tip. The orifice geometry was obtained from direct measurement of the valve tip and receiver. An approximate range of motion of the valve tip was also obtained from these direct measurements. The dynamic characteristics, on the other hand, were obtained by isolating the servovalve from the actuator by immobilizing the load with the brace. Since the valve tip position is not measurable, it is expressed in terms of the load pressure, that is,

$$x_v = f\left(P_{load}\right) = K_v P_{load} \tag{15}$$

Here, $K_v$, is the inverse of the slope of the load pressure/valve tip position static characteristic. The slope is taken as constant. Neglecting flow forces, the valve tip dynamic equation (4) can be rewritten as a relation between the input current after hysteresis and the load pressure

$$\begin{aligned} \ddot{x}_v + 2\zeta_P \omega_{nP} \dot{x}_v + \omega_{nP}^2 x_v &= \frac{B}{m_v} i_{hys} \\ \ddot{P}_{load} + 2\zeta_P \omega_{nP} \dot{P}_{load} + \omega_{nP}^2 P_{load} &= \frac{B}{m_v K_v} i_{hys} \end{aligned} \tag{16}$$

This can be written in transfer function form as

$$\frac{P_{load}}{i_{hys}} = \frac{K_{dc}\omega_{nP}^2}{s^2 + 2\zeta_P \omega_{nP} s + \omega_{nP}^2} \tag{17}$$

For this system, the damping ratio, natural frequency and the DC gain, $K_{dc}$, will depend on the input current. However, for simplicity, it is assumed that the damping ratio and the natural frequency are constant. A reasonable relationship between the DC gain and the valve tip position was obtained for best correspondence with experimental data. It is in $K_{dc}$ that any nonlinearities in the servovalve parameters or in the discharge coefficients are lumped. The gain was determined from experimentally determined Bode plots. It was found that the DC gain between the load pressure and input current decreases with increasing amplitude of current.

**3.2.2: Shaft Stiffness.** The joint shaft stiffness was obtained by immobilizing the elbow joint and measuring torque and angular motor position. Plotting torque versus angular position an approximate straight line results whose slope is the angular joint stiffness, given in Figure 3. After a series of tests, an average joint stiffness was found to be $8.9\times10^4$ *lb·in/rad* ($10.05\times10^3$ *N·m/rad*). Theoretically, assuming a solid shaft, the shaft stiffness is approximately given by

$$k_s = \frac{GJ}{l_s} = 11.06\times10^4 \frac{lb\cdot in}{rad}\left(12.50\times10^3 \frac{N\cdot m}{rad}\right) \tag{18}$$

where, $G$ is the shear modulus of the shaft material, $J$ is the shaft moment of inertia and $l_s$ is the shaft length.

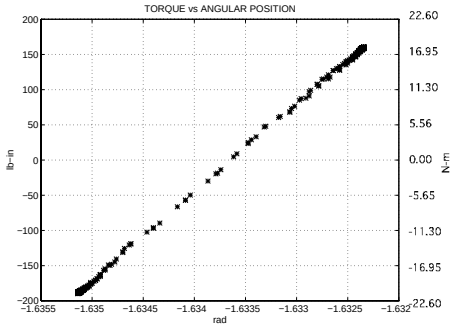


**Figure 3. Determination of Shaft Stiffness.**

**3.2.3: Volumetric Displacement.** Another key parameter is the actuator volumetric displacement, $D_v$, since it relates the load flow to the angular velocity and the load pressure to the joint torque. These relations are given by

$$Q_{load} = D_v \omega_{vn}, \text{ and } P_{load} = \frac{\tau}{D_v} \tag{19}$$

With the manifold installed and the elbow free to rotate, a sinusoidal current was sent in open-loop resulting in an

oscillation of the arm. With torque and pressure measurements, the torque vs load pressure was plotted as shown in Figure 4. Here, the slope of the inclined line segments is close to the ideal volumetric displacement of the rotary actuator, assuming external leakage of the actuator is small. The slope is found as $D_v$ = 0.288 $in^3$/rad (4.72 $cm^3$/rad). The horizontal portions of the curve in Figure 4 are due to the friction within the rotary actuator. The difference between the measured torque and the applied torque from pressure measurements was used to identify the Coulomb friction. Since the pressure measurements do not include friction and the torque measurements do, the difference between the two is due to stick-slip phenomenon and allows a good approximation of the Coulomb friction. Continuing, the actuator leakage between chambers can be found, with the elbow immobilized and pressures measured. The actuator leakage coefficient, $R_v$, is taken as a constant and it was estimated to be $8.24\times10^{-5}$ $in^5/lb\text{-}s$ ($1.96\times10^{-7}$ $m^3/MPa\text{-}s$).

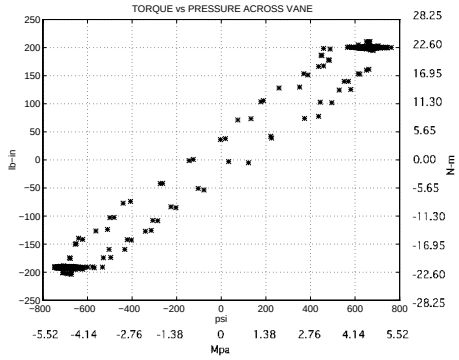


**Figure 4. Determination of Actuator Volumetric Displacement.**

As for the load parameters, they were obtained by a least squares estimation. In the case of the mass of the load, it was verified under static conditions also. Parameters that were not estimated with good certainty include clearance between valve tip and receiver. In these cases, these parameters were tuned until a satisfactory correlation between simulation and experiments was obtained.

## 4: Validation

To test how well the model can predict system behavior, experiments and simulations were compared. The *s-function* approach in Matlab with Gear integration method was used. Experiments were performed in open loop mode at an operating supply pressure of 3000 *psi* (20.7 *Mpa*). Results were sampled at 10 *ms*. The model was validated for the static case in a previous paper, [1], and for other frequencies and amplitudes although not shown here.

### 4.1: Servovalve Dynamics

In order to verify the servovalve model, experiments and simulations were done for the case of a locked joint. This, in effect, isolates the servovalve dynamics from load dynamics allowing the validation of the servovalve model. In simulation, the vane and load positions and their derivatives were constrained to be zero. Simulation initial conditions were set to match those of the experiments. Before the execution of the experiments, a decaying sinusoidal current allowed the response to begin with a load pressure of close to zero, resulting in a valve tip position practically at the null.

For sinusoidal currents of amplitudes 0.2A and 0.3A and frequency of 1.0 *rad/s*, the supply pressure and the two chamber pressures are shown in Figure 5 and Figure 6, respectively. The model is able to predict quite well the pressure response, which is sufficient for control purposes.

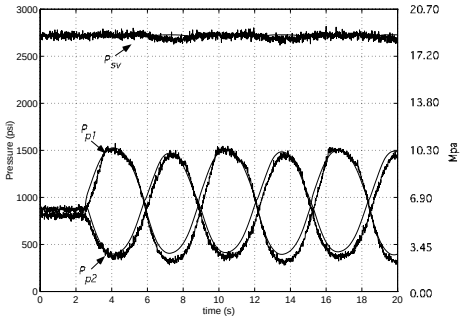


**Figure 5. Supply and Chamber Pressures, Current Amplitude of 0.2 A.**

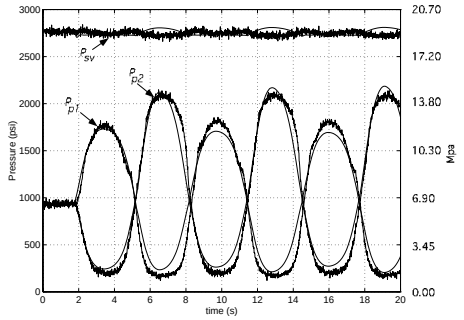


**Figure 6. Supply and Chamber Pressures, Current Amplitude of 0.3 A.**

### 4.2: Overall Joint Dynamics

In this section, the overall joint model is verified. Experiments and simulations were done for the case with the joint free to rotate. For an input current given as

$$i = 0.1\sin(0.25t) \qquad (20)$$

the pressures are plotted with respect to time in Figure 7. Of importance in force control is the load pressure, which is plotted in Figure 8. Results show that the model predicts

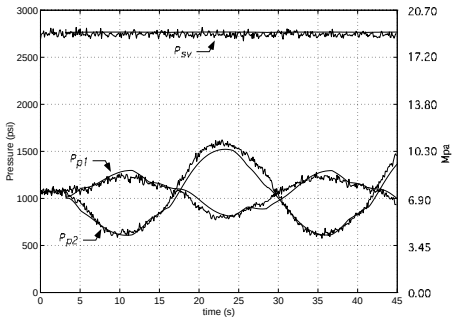


**Figure 7. Supply and Chamber Pressures: No brace.**

well the pressure response. The response of the load position, illustrated in Figure 9, compares well to the experimental load position. As the arm approaches the highest parts of its trajectory, the stick-slip friction model is satisfactory. Overall, the model predicts well the load angular position.

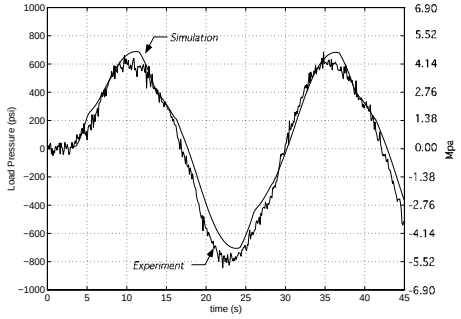


**Figure 8. Load Pressure: Experiment and Simulation.**

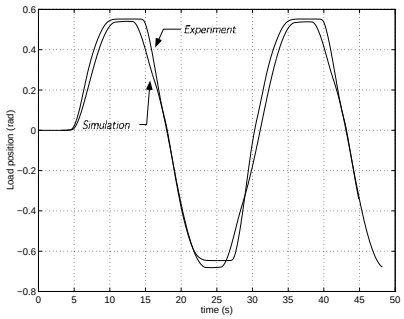


**Figure 9. Load Position: Experiment and Simulation.**

Some differences between simulation and experiments do exist due to unmodelled effects and due to the lumped parameter approach in modelling. Some of the these factors include temperature variation of oil properties, and losses in the numerous elbows and fittings in the oil passages. However, as the above results indicate, they do not seem to be significant for the purpose of control and therefore no further modelling of these effects is required.

## 5: Conclusions

An accurate model of a hydraulic joint of a manipulator has been presented. The model follows closely experimental results. The model accounts for the major effects of an electrohydraulic actuator such as hysteresis, flow through orifices, and line losses. In addition, even though access to the servovalve is limited, the model is able to characterize the servovalve dynamics well. The developed model represents well the behavior of the real system and can be extended to other joints of the SARCOS slave manipulator as well as the master in such a way as to obtain a complete model of the hydraulics of the SARCOS manipulator. For control purposes, a reduced-order model which will capture the major dynamics of the system will be called upon. It is expected that this model will be useful in designing a robust force controller in order to reduce control effort and to improve control performance.

## Acknowledgments

The support of this work by the Fonds pour la Formation de Chercheurs et l'Aide à la Recherche (FCAR), and by the Natural Sciences and Engineering Council of Canada (NSERC) is gratefully acknowledged.

## References

[1] Bilodeau, G., and Papadopoulos, E., "Development of a Hydraulic Manipulator Servoactuator Model: Simulation and Experimental Validation," *IEEE Int. Conf. on Robot. and Autom.*, pp. 1547-1552, 1997.

[2] Blackburn, J.F., Reethof, G., and Shearer, J.L., ed. *Fluid Power Control*, Cambridge: M.I.T. Press, 1960.

[3] Bluethmann, B., et. al., "Experiments in Dexterous Hybrid Force and Position Control of a Master/Slave Electrohydraulic Manipulator," *IEEE/RSJ Int. Conf. on Intell. Robots and Syst.*, Vol. 3, pp. 27-32, 1995.

[4] Boulet, B., et. al., "Characterization, Modeling and Identification of a High Performance Hydraulic Actuator for Robotics," *Centre for Intelligent Machines report TR-CIM-93-9*, McGill University, March 1993.

[5] Carpenter, K.H., "A Differential Equation Approach to Minor Loops in the Jiles-Atherton Hysteresis Model," *IEEE Trans. on Magnetics*, Vol. 27, No. 6, pp. 4404-4406, 1991.

[6] Dunnigan, M.W., et. al., "Hybrid Position/Force Control of a Hydraulic Underwater Manipulator," *IEE Proc.: Control Theory and Appl.*, Vol. 143, No. 2, pp. 145-151, March 1996.

[7] Habibi, S.R., Richards, R.J., and Goldenberg, A.A., "Hydraulic actuator analysis for industrial robot multivariable control," *Proc. of the Am. Control Conf.*, (Baltimore, Maryland), pp. 1003-1007, 1994.

[8] Heinrichs, B., Sepehri, N., and Thornton-Trump, A.B., "Position-Based Impedance Control of an Industrial Hydraulic Manipulator," *IEEE Int. Conf. on Robot. and Autom.*, pp. 284-290, 1996.

[9] Heintze, J., et. al., "Modeling and control of an industrial hydraulic rotary vane actuator," *Proc. of the 32nd Conf. on Decis. and Control*, (San Antonio, Texas), pp. 1913-1918, December 1993.

[10] Kwon, D.S., et. al., "Tracking Control of the Hydraulically Actuated Flexible Manipulator," *IEEE Int. Conf. on Robot. and Autom.*, pp. 2200-2205, 1995.

[11] Laval, L., M'Sirdi, N.K., and Cadiou, J-C., "$H_\infty$-Force Control of a Hydraulic Servo-Actuator with Environmental Uncertainties," *IEEE Int. Conf. on Robot. and Autom.*, pp. 1566-1571, 1996.

[12] McLain, T.W., et. al., "Development, Simulation, and Validation of a Highly Nonlinear Hydraulic Servosystem Model," *Proc. of the Am. Control Conf.*, (Pittsburgh, Pennsylvania), pp. 385-391, June 1989.

[13] Merrit, H.E., *Hydraulic Control Systems*, New York: John Wiley and Sons Inc., 1967.

[14] Unruh, S., et. al., "A hybrid position/force and positional accuracy controller for a hydraulic manipulator," *SPIE Telemanipulator and Telepresence Technol.*, vol.2351, pp. 207-213, 1994.